Laboratory Infrared Observation of Linear C_7S Carbon−Sulfur Cluster in Solid Argon

Haiyan Wang, Jan Szczepanski, Philip J. Brucat, and Martin T. Vala*

Department of Chemistry and Center for Chemical Physics, University of Florida, Gainesville, Florida 32611-7200

Received: June 13, 2003

The linear carbon−sulfur cluster C_7S has been generated by pulsed laser evaporation of a carbon/sulfur mixture, deposited in an argon matrix at 12 K, and studied by Fourier transform infrared spectroscopy. Three new vibrational bands at 2088.1, 1913.6, and 1256.1 cm^{-1} have been observed. Using density functional and ab initio theoretical methods, these three bands have been assigned to the $\nu_2(\sigma)$, $\nu_3(\sigma)$, and $\nu_5(\sigma)$ fundamental stretching modes, respectively, of linear C_7S. These assignments have been confirmed by ^{13}C isotopic shifts. Possible formation mechanisms of C_7S in a matrix via addition reactions of C, S, and CS species to the already-formed C_nS and C_n carbon−sulfur and carbon clusters are suggested. Finally, vibrational frequencies for the series of linear clusters C_nS ($n = 1-9$) have been calculated at the B3LYP/cc-pVDZ level and compared with available experimental data.

I. Introduction

Because of their involvement in interstellar chemistry and in material science, small carbon−sulfur clusters have been the subject of substantial current research. The C_nS ($n = 1-3, 5$) species have been observed in the envelopes of several stars, such as TMC-1 and IRC+10216.[1−4] Absence of an electric dipole precludes the interstellar detection of the symmetric SC_nS species via microwave detection methods, although they are probably also present in circumstellar regions. Carbon−sulfur systems are also attractive from a material science point of view because small C_nS_m species have been found to possess unusual electrical properties.[5]

A number of sulfur-containing carbon clusters have been produced in the laboratory. C_nS ($n = 1, 3$) and C_nS_2 ($n = 2-6$) clusters have been obtained by pyrolysis or by electrical discharge and investigated by neutralization−reionization mass spectrometry.[6−11] C_nS and C_nS_2 ($n = 1-5$) clusters have also been generated by laser ablation. Some have been identified in our laboratory[12] by FT-IR spectroscopy complemented by density functional theory (DFT) calculations. Rotational constants for linear C_nS ($n = 1-9$) species have been determined by several groups.[13−17] Although early theoretical work focused on the smaller species ($n = 1-9$),[18−25] Pascoli and Lacendy recently computed DFT spectroscopic parameters for carbon−sulfur clusters up to $C_{20}S$.[26] They found that the C_nS cluster chains terminated by a S atom are linear, except for $C_{18}S$, which was predicted to have a monocyclic structure containing the sulfur atom equally bonded to two adjacent carbons. Subsequent work on C_nS and C_nS_2 clusters confirmed the linear structure of these species.[27−29]

The present paper is focused on the neutral linear C_7S cluster. C_7S was produced by the vaporization of a carbon and sulfur mixture, and studied via FT-IR spectroscopic methods in argon matrices. Isotope shifts were also investigated. DFT and ab initio calculations were used to identify three new vibrational modes. Its energy, structural parameters, and vibrational frequencies have been computed using DFT and other methods.

II. Computation Details

All calculations are carried out using the GAUSSIAN 98 suite of programs.[30] On the basis of previous work, the C_7S cluster was assumed initially to be linear, with sulfur at one end.[6−29] Geometry optimization was effected using DFT/ B3LYP theory with Dunning's correlation consistent double ξ (cc-pVDZ) basis set.[31] Geometries, frequencies, and isotope shifts were also calculated at other levels of theory, but little difference was found. The geometry of C_7S was also calculated with no assumption of linearity. A bent structure in the ground $^1A'$ state was determined, but this structure was very close to linear and had a higher energy than the linear form. Finally, MP2 and CCSD(T) methods were used, but invariably led to a different electronic state with a lower rotational constant than found experimentally.

III. Experimental Methods

C_7S was generated by laser ablation of pressed pellets of ^{12}C (powdered graphite, natural abundance ^{12}C (98.9%) and ^{13}C (1.1%); ^{13}C (99%, Cambridge Isotope Laboratories, Inc.)), and S (natural abundance ^{32}S (96%) and ^{34}S (4%)) using a pulsed Nd:YAG laser (1064 and 532 nm). The reaction products were trapped with Ar isolant gas on a CsI window cooled to 12 K by a closed-cycle helium cryostat (ADP Displex). Secondary reactions were noted after annealing of the matrix (to 35 K). Infrared absorption spectra were recorded with a Nicolet Magna 560 Fourier transform infrared (FT-IR) spectrometer in the 700−7000 cm^{-1} region at 0.25 cm^{-1} resolution.

IV. Theoretical Predictions

In its $^1\Sigma^+$ ground-state linear C_7S has 34 valence electrons, 16 of which are distributed in 8 doubly degenerate π orbitals. Table 1 lists the C_7S state energies, dipole moment, bond lengths, rotational constant, and vibrational frequencies, obtained at various levels of theory. Although primarily cumulenic in

* To whom correspondence should be addressed. E-mail: mvala@chem.ufl.edu.

10.1021/jp030752q CCC: $25.00
Published on Web 11/21/2003

TABLE 1: Energies E_n (Hartrees), Zero Point Energies ZPE (kcal/mol), Dipole Moments μ_e (Debyes), Bond Lengths (Å), Rotational Constants B_e (GHz), Harmonic Vibrational Frequencies ω (unscaled, cm^{-1}), and Integral IR Intensities (km/mol, in Parentheses), Calculated for Linear C_7S at Various Levels of Theory

C_7S	B3LYP/6-311G*	B3LYP/cc-pVDZ	B3LYP/aug-cc-pVTZ	CASSCF(4,6)/cc-pVDZ
E	−664.7483	−664.6965	−664.7887	−662.3804
ZPE	20.3672	21.7178	20.9487	22.3260
μ_e	5.7301	5.7005	6.1616	5.8285
S—C_1	1.5579	1.5668	1.5542	1.5454
C_1—C_2	1.2779	1.2875	1.2764	1.2780
C_2—C_3	1.2699	1.2799	1.2675	1.2635
C_3—C_4	1.2811	1.2905	1.2795	1.2894
C_4—C_5	1.2656	1.2755	1.2625	1.2680
C_5—C_6	1.2929	1.3022	1.2915	1.2989
C_6—C_7	1.2817	1.2911	1.2763	1.2658
B_e[a]	0.4141	0.4081	0.4156	0.4149
B_e[b]	0.4042	0.3984	0.4057	0.4050
$\omega_1(\sigma)$	2229.8 (231)	2238.6 (799)	2218.9 (339)	2339.0
$\omega_2(\sigma)$	2209.2 (5750)	2223.3 (5089)	2191.2 (5956)	2295.5
$\omega_3(\sigma)$	2009.8 (2859)	2018.5 (2607)	2003.8 (3107)	2054.5
$\omega_4(\sigma)$	1712.4 (139)	1719.2 (93)	1710.5 (141)	1811.7
$\omega_5(\sigma)$	1284.8 (284)	1289.7 (236)	1284.5 (259)	1368.6
$\omega_6(\sigma)$	854.9 (86)	858.3 (75)	855.7 (90)	901.5
$\omega_7(\sigma)$	431.9 (3)	433.7 (3)	432.5 (3)	458.0
$\omega_8(\pi)$[c]	615.2 (6)	700.3 (6)	573.1 (5)	669.7
$\omega_9(\pi)$[c]	449.7 (1)	577.2 (0)	522.7 (0)	591.6
$\omega_{10}(\pi)$[c]	308.4 (4)	453.5 (1)	445.7 (0)	500.3
$\omega_{11}(\pi)$[c]	233.2 (0)	268.7 (3)	246.4 (2)	240.0
$\omega_{12}(\pi)$[c]	118.7 (8)	150.5 (4)	138.9 (4)	140.3
$\omega_{13}(\pi)$[c]	31.5 (0)	55.0 (2)	51.4 (2)	52.2

[a] Experimental rotational constant for C_7S is 0.4144 GHz.[17] [b] Rotational constant for $C_7{}^{34}S$; experimental constant is 0.4045 GHz.[17] [c] Doubly degenerate bending (π) modes.

TABLE 2: Energies E_n (Hartrees), Dipole Moments μ_e (Debyes), Bond Lengths (Å), and Rotational Constants B_e (GHz), Calculated for Linear C_7S at Various Levels of Theory, All with a cc-pVDZ Basis Set

C_7S ($^1\Sigma^+$)	MP2	CCSD(Full)	QCISD(T)	CCSD(T)	CCSD(T)(Full)
E	−663.3229	−663.3265	−663.3863	−663.3829	−663.4050
μ_e	5.0215	5.4842	4.4692	4.6856	4.7090
S—C_1	1.5701	1.5622	1.5806	1.5776	1.5758
C_1—C_2	1.3041	1.2982	1.3009	1.3018	1.3006
C_2—C_3	1.2904	1.2818	1.2958	1.2938	1.2927
C_3—C_4	1.3045	1.3013	1.3031	1.3042	1.3029
C_4—C_5	1.2882	1.2789	1.2926	1.2908	1.2897
C_5—C_6	1.3162	1.3130	1.3156	1.3165	1.3152
C_6—C_7	1.3104	1.2964	1.3138	1.3118	1.3107
B_e[a]	0.4005	0.4050	0.3990	0.3995	0.4005

[a] Experimental rotational constant for C_7S is 0.4144 GHz.[17] Note that the predicted B_e values are in poorer agreement with experiment than the B_e values calculated at the B3LYP and CASSCF(4,6) levels listed in Table 1.

bonding, C_7S still shows a small alternation in its C—C bond lengths, a fact previously noted for smaller C_nS ($n = 1-5$) clusters.[12] For example, the C_4—C_5 bond length in C_7S is shorter than the C_3—C_4 bond length (by ca. 0.016 Å). Different methods and basis sets predict similar carbon−carbon bond lengths and show the same alternation. The average C—C bond length is about 1.28 Å, which is close to the experimental value and also close to other theoretical results. The calculated C—S bond length, however, appears to vary with theoretical approach. In C_5S, this bond length is about 1.547(6) Å.[17] Because of the similarities with other C_nS clusters,[24] it is expected that in C_7S it should be close to 1.55 Å. Determining the C−S bond length through the effect of isotopic substitution on the rotational constant is model dependent (cf., Table 1).

Although both B3LYP and CASSCF (4, 6) methods predict the structure of C_7S reliably, it was also studied by the CCSD-(T) and MP2 methods. The theoretical state energies, zero point energies (ZPEs), bond lengths, and rotational constants are listed in Table 2. The rotation constants obtained by CCSD(T) calculations are worse than those using DFT, despite the fact that it provides for precise electronic correlation.

As a test of the stability of the ground-state wave function an EOM-CCSD (Aces II)[32] calculation was performed on C_7S with the same basis set and geometry as in the B3LYP calculations. Because only positive excitation energies were found, it was concluded that the predicted structural and spectroscopic constants found at the B3LYP/cc-pVDZ level should be reliable.

Theoretical vibrational frequencies can often be used to identify new molecular species. Table 3 presents the results of our B3LYP/cc-pVDZ level calculations on two carbon−sulfur cluster series, some members of which have not yet been observed. For clusters that have been observed, comparison of the calculated frequencies (with appropriate scaling factors, cf. Table 3) with the predicted vibrational frequencies shows reasonably good agreement. The maximum discrepancy in the C_nS series was found for the ν_5 mode of C_7S (ca. 30 cm^{-1}), whereas the worst discrepancy in the SC_nS series was found for the ν_5 mode of SC_5S (ca. 27 cm^{-1}). These discrepancies arise either from mixing of similar modes not explicitly considered or from the uniform scaling used for all C—C and C—S vibrational frequencies. For instance, the ν_5 mode of C_7S

TABLE 3: Comparison of Experimental (Ar Matrix) and Calculated (B3LYP/cc-pVDZ) Most Intense IR Mode Frequencies (cm^{-1}) for Linear C_nS ($n = 1-9$) and SC_nS ($n = 1-9$) Carbon−Sulfur Clusters in Their Electronic Ground States (Relative Intensities in Parentheses)

C_nS	mode	ν_{exp} (cm^{-1})	ν_{cal}[a] (cm^{-1})	SC_nS	mode	ν_{exp} (cm^{-1})	ν_{cal}[a] (cm^{-1})
CS ($^1\Sigma^+$)	ν_1 (σ); C−S	1275.1 (1.0)[c,d]	1275.1 (1.0)	SCS ($^1\Sigma_g^+$)	ν_2 (σ_u); C−S	1528.2 (1.0)[c,d]	1533.9 (1.0)
C_2S ($^3\Sigma^-$)	ν_1 (σ); C−C		1636.2 (1.0)	SC_2S ($^3\Sigma_g^-$)	ν_3 (σ_u); C−S	1179.7 (1.0)[d]	1159.3 (1.0)
C_3S ($^1\Sigma^+$)	ν_1 (σ); C−C	2047.6 (1.0)[c,d]	2047.6 (1.0)	SC_3S ($^1\Sigma_g^+$)	ν_3 (σ_u); C−C	2078.5 (1.0)[c,d]	2081.5 (1.0)
	ν_2 (σ); C−S	1533.2 (0.1)[d]	1540.8 (0.04)		ν_4 (σ_u); C−S	1024.6 (0.18)[c,d]	1022.7 (0.11)
	ν_3 (σ); C−S	725.6 (0.009)[d]	726.6 (0.009)				
C_4S ($^3\Sigma^-$)	ν_2 (σ); C−C	1746.8 (1.0)[c]	1727.3 (1.0)	SC_4S ($^3\Sigma_g^-$)	ν_4 (σ_u); C−C	1872.1 (1.0)[d]	1855.0 (1.0)
					ν_5 (σ_u); C−S	897.7 (0.117)[d]	870.3 (0.18)
						843.7 (0.056)[d]	
C_5S ($^1\Sigma^+$)	ν_1 (σ); C−C	2124.5 (1.0)[c]	2140.0 (1.0)	SC_5S ($^1\Sigma_g^+$)	ν_4 (σ_u); C−C	2104.7 (1.0)[d]	2118.5 (1.0)
	ν_3 (σ); C−C		1580.0 (0.15)		ν_5 (σ_u); C−C	1687.9 (0.36)[d]	1661.2 (0.24)
					ν_6 (σ_u); C−S	783.5 (0.04)[d]	796.4 (0.04)
C_6S ($^3\Sigma^-$)	ν_2 (σ); C−C		1995.4 (1.0)	SC_6S ($^3\Sigma_g^-$)	ν_5 (σ_u); C−C		2031.5 (1.0)
	ν_4 (σ); C−C		1344.8 (0.18)		ν_6 (σ_u); C−C		1458.4 (0.29)
C_7S ($^1\Sigma^+$)	ν_2 (σ); C−C	2088.1 (0.67)[b,e]	2114.5 (1.0)	SC_7S ($^1\Sigma_g^+$)	ν_5 (σ_u); C−C		2088.5 (1.0)
	ν_3 (σ); C−C	1913.6 (1.0)[b]	1919.7 (0.51)		ν_6 (σ_u); C−C		1952.7 (0.88)
	ν_5 (σ); C−C	1256.1 (0.07)[b]	1226.6 (0.05)		ν_7 (σ_u); C−C		1341.4 (0.14)
C_8S ($^3\Sigma^-$)	ν_1 (σ); C−C		2072.2 (1.0)	SC_8S ($^3\Sigma_g^-$)	ν_6 (σ_u); C−C		2073.8 (1.0)
	ν_4 (σ); C−C		1760.6 (0.43)		ν_7 (σ_u); C−C		1822.6 (0.48)
	ν_6 (σ); C−C		1092.9 (0.06)		ν_8 (σ_u); C−C		1211.5 (0.16)
C_9S ($^1\Sigma^+$)	ν_2 (σ); C−C		2099.1 (0.09)	SC_9S ($^1\Sigma_g^+$)	ν_7 (σ_u); C−C		1994.3 (1.0)
	ν_3 (σ); C−C		2019.5 (1.0)		ν_8 (σ_u); C−C		1697.5 (0.14)
	ν_5 (σ); C−C		1658.3 (0.095)		ν_9 (σ_u); C−C		1127.8 (0.04)

[a] Scaled uniformly by 0.9510 factor for modes with primarily C−C character and by 0.9824 factor for modes with primarily C−S character. [b] This work. [c] Reference 12. [d] References 6, 8−9, 11. [e] Tentative assignment.

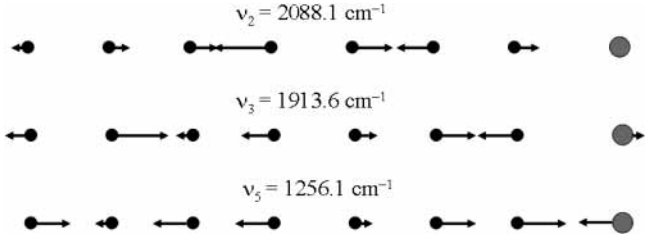

Figure 1. Schematic representation of the atomic motion in the $\nu_2(\sigma)$, $\nu_3(\sigma)$, and $\nu_5(\sigma)$ fundamental vibrational modes of linear C_7S.

is primarily a C—C stretching mode, but the C—S vibration also contributes to this mode. Because the common scaling factor used for these modes does not account for this mixing, the scaled ν_5 frequency does not match the experimental value very well.

Because no imaginary frequencies were found for C_7S (cf. Table 1), its linear geometry is associated with a local minimum on the potential energy surface. Calculations at different levels all predict similar vibrational frequencies for C_7S. Its seven stretching (σ) modes and six doubly degenerate bending (π) modes are all infrared active. Generally, σ modes exhibit high intensities whereas π modes possess relatively low intensities. Because the values of ω_1 and ω_2 are very close, a mixture of these two modes via Fermi resonance is possible. Isotopic shift calculations reveal that the intensity of the ω_2 mode is redistributed into the ω_1 mode, which makes it difficult to predict the integral intensity of the ω_2 mode solely from theoretical calculations.

Mode mixing could explain the fact that although the most intense mode calculated for C_7S is ν_2, the ν_3 mode is the strongest observed. The ratio of experimental integral intensities for the ν_3 and ν_5 modes is ca. 14.3, of the same order of magnitude as the computed values of 10.0 (B3LYP/6-311G*), 11.0 (B3LYP/cc-pVDZ), and 12.0 (B3LYP/aug-cc-pVTZ); cf. Table 1. But, the analogous ratio for the ν_2 and ν_3 modes is 0.67, much smaller than the calculated ratios of 2.01, 1.95, and 1.92, respectively (cf. Table 1).

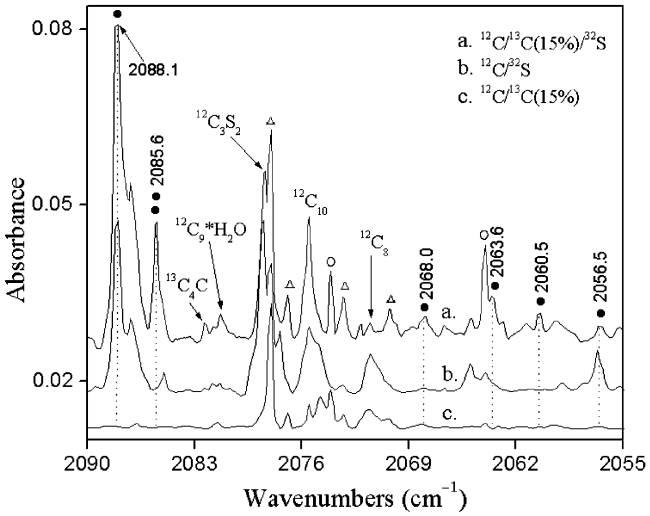

Figure 2. IR absorption spectrum of the $\nu_2(\sigma)$ mode region of neutral C_7S and its ^{13}C isotopic partners produced by laser ablation of a 1.0:0.15:1.0 mixture of ^{12}C:^{13}C:^{32}S isolated in an Ar matrix at 35 K. Two other spectra for $^{12}C/^{32}S$ and $^{12}C/^{13}C$ mixtures under the same experimental conditions are included to confirm the band assignments. All-^{12}C and singly-^{13}C substituted isotopomeric bands are marked with dots. Overlapped bands are marked with two dots. Bands marked by empty triangles and circles are assigned to $^{12/13}C_9$ and $^{12}C_n$ clusters, respectively.

V. Results

Three new bands have been observed at 2088.1, 1913.6, and 1256.1 cm^{-1}, assigned here to the ν_2 , ν_3, and ν_5 stretching modes of linear C_7S, respectively; cf. Figure 1. Figure 2 shows the infrared spectrum of the ν_2 mode for neutral C_7S and its ^{13}C isotopic partners (from a $S/^{13}C$ mixture). Two other spectra for $^{12}C/^{32}S$ and $^{12}C/^{13}C$ mixtures, under the same experimental conditions, are also included and confirm these assignments. Trapping the products (in solid Ar, ca. 12 K) and annealing (to 35 K), leads to the IR spectra (in Figure 3) of the C_7S ν_2 mode and its ^{13}C isotopomeric bands. The corresponding spectra for the ν_3 and ν_5 modes are presented in Figures 4, 5 and 6, 7,

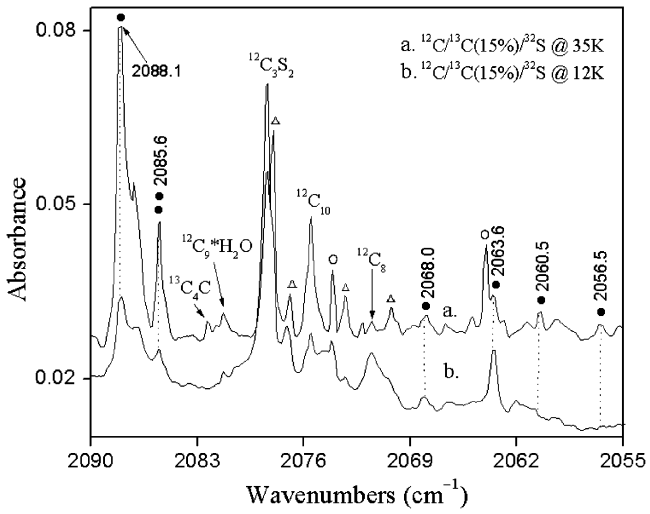

Figure 3. IR absorption spectra of the $\nu_2(\sigma)$ mode region of neutral C_7S and its ^{13}C isotopic partners recorded after trapping the products in Ar at ca. 12 K, followed by annealing at 35 K.

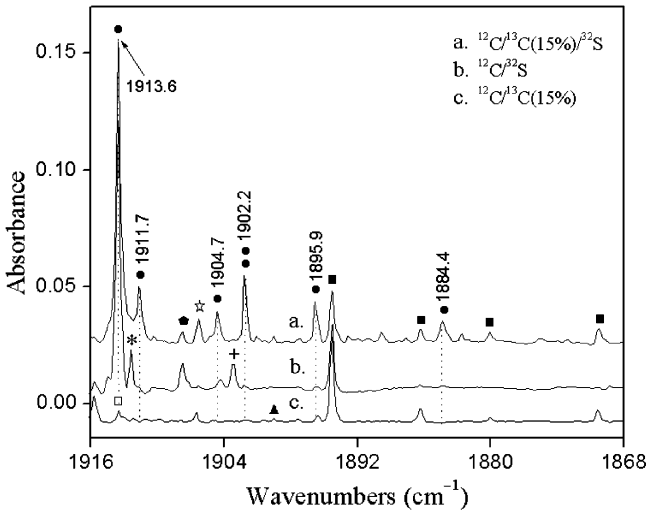

Figure 4. IR absorption spectrum of the $\nu_3(\sigma)$ mode region of neutral C_7S and its ^{13}C isotopic partners produced by laser ablation of a 1:0.15:1 mixture of ^{12}C:^{13}C:^{32}S in an Ar matrix at 35 K. Two other spectra for $^{12}C/^{32}S$ and $^{12}C/^{13}C$ mixtures under the same experimental conditions are shown to confirm the band assignments. All-^{12}C and singly-^{13}C substituted isotopomeric bands are marked with dots, and overlapped bands are marked by two dots. Peaks with filled squares are due to all-^{12}C and singly-^{13}C substituted of linear C_7. Bands marked by an empty square, black pentagon, empty star, plus sign and black triangle are assigned to 12-13-13-12-12-12 ($^{12/13}C_6$), $^{12}C_nS_m$, $^{13}C_n$, $^{12}C_nS_m$, and $^{13}C_n$ clusters, respectively.

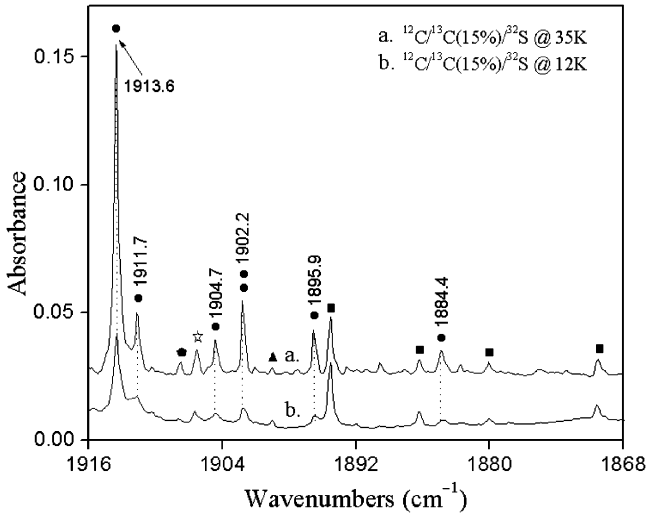

Figure 5. IR absorption spectra of the $\nu_3(\sigma)$ mode region of neutral C_7S and its ^{13}C isotopic partners recorded after trapping the products in Ar at ca. 12 K, followed by annealing at 35 K.

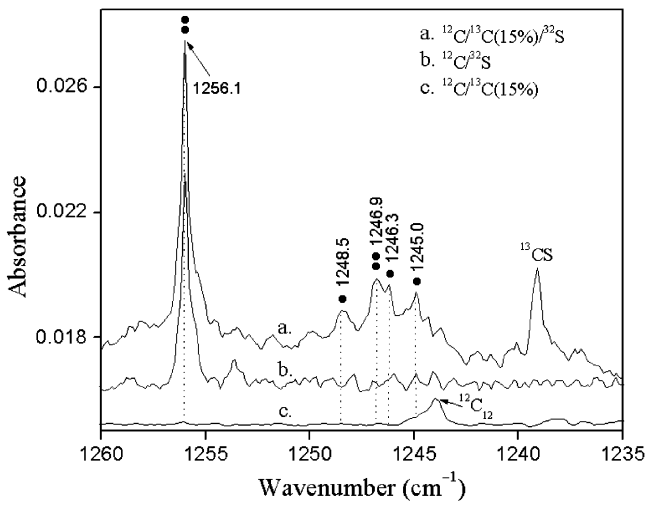

Figure 6. IR absorption spectrum of the $\nu_5(\sigma)$ mode region of neutral C_7S and its ^{13}C isotopic partners produced by laser ablation of a 1.0:0.15:1.0 mixture of ^{12}C:^{13}C:^{32}S isolated in an Ar matrix at 35 K. Two other spectra for $^{12}C/^{32}S$ and $^{12}C/^{13}C$ mixtures under the same experimental conditions are included to confirm the band assignments. All-^{12}C and singly-^{13}C substituted isotopomeric bands are marked with dots, and overlapped bands are marked with two dots.

respectively, where band assignments to pure carbon or other small carbon sulfur clusters are indicated.[12,33−35] For example, the 1244.0 cm^{-1} band (cf. Figure 6c) is due to the ν_{10} (σ_u) mode of $^{12}C_{12}$ ($X^3\Sigma_g$), on the basis of recent work.[35] Each new assignment is discussed in turn below.

A. Band Assignment for the $\nu_2(\sigma)$ Vibration. Frequency calculations for the ν_2 mode of C_7S gave 2114.5 cm^{-1} (cf., Table 3). With an assumed calculation error of ±50 cm^{-1}, an observed band at 2088.1 cm^{-1} has been assigned tentatively to this mode. Several reasons account for this attribution. First, experiments under different conditions (such as matrix temperature and/or laser photon flux) showed that this band tracked the intensities of the two bands (1913.6 and 1256.1 cm^{-1}) also assigned to linear C_7S (vide infra). Second, of the small and mid-sized C_nS and SC_nS clusters given in Table 3, the 2088.1, 1913.6, and 1256.1 cm^{-1} bands fit only the frequency pattern predicted for C_7S. However, as stated earlier, the mixing of ν_1 and ν_2 modes can lead to uncertainties in the predicted intensities and frequencies of the all-^{12}C and its single ^{13}C substituted isotopomers. In fact, in the **13**-12-12-12-12-12-12-32, 12-12-12-12-12-**13**-12-32, and 12-12-12-12-12-12-**13**-32 isotopomers, which show the largest deviations in difference frequency values (i.e., $\nu_{exp} - \nu_{cal}$), there is a very large intensity flow from the ν_2 to the ν_1 mode. Therefore, the 2085.6 and 2063.6 cm^{-1} band assignments for the ν_2 mode in these isotopomers (in Figures 2 and 3 and Table 4) are considered tentative. The annealing spectra of Figure 3 support this statement.

An analysis of the spectra in Figures 2 and 3 raises the question: why is the intensity of the 2085.6 cm^{-1} band as intense as it is relative to the 2088.1 cm^{-1} band? The carrier of this band could be a singly ^{13}C substituted isotopomer of $^{12/13}C_nS$, a $^{12/13}C_nS_2$ cluster, or a doubly ^{13}C substituted group of similar clusters, all of which might have a frequency close to 2085 cm^{-1}. If only cluster sizes with $n < 10$ are considered,

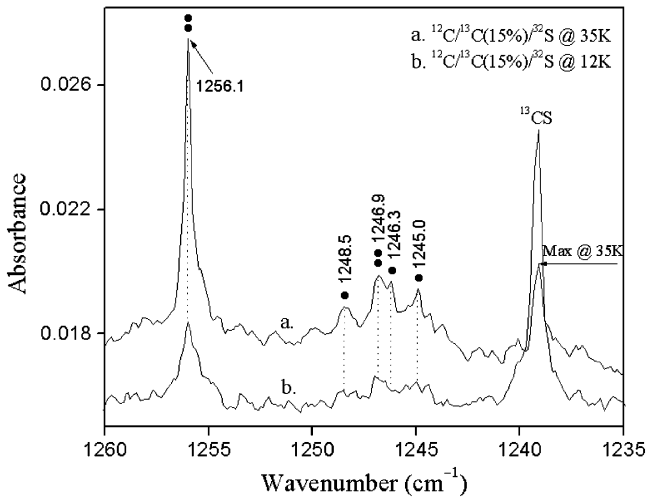

Figure 7. IR absorption spectra of the $\nu_5(\sigma)$ mode region of neutral C_7S and its ^{13}C isotopic partners recorded after trapping the products in Ar at ca. 12 K, followed by annealing at 35 K.

calculations show none of these possibilities are tenable. One further possibility is some band intensity comes from the ν_1 mode of some singly ^{13}C substituted isotopomers of $^{12/13}C_7S$. The B3LYP/cc-pVDZ (unscaled) frequencies (with intensities in parentheses) of the **13**-12-12-12-12-12-12-32, 12-12-12-12-**13**-12-32, and 12-12-12-12-12-12-**13**-32 isotopomers are 2235.7 (900), 2234.2 (3400), and 2234.1 cm^{-1} (2220 km/mol). When grouped together, these bands have a total integral intensity comparable to the ν_2 mode of $^{12}C_7S$ (cf. Table 1). A 0.9335 scaling factor fits these calculated frequencies to the 2085.6 cm^{-1} experimental band well (cf. Figure 2).

Considering all the above difficulties in determining the singly ^{13}C substituted isotopomer frequencies and intensities, the assignment of the 2088.1 cm^{-1} band to the ν_2 mode of C_7S must be considered tentative.

B. Isotopomer Band Assignments for the $\nu_3(\sigma)$ Vibration. In the past the absorption at 1913.6 cm^{-1} has been assigned to the ν_4 mode of the 12-**13**-**13**-12-12-12 isotopomer of C_6 (Figure 4c). There are, however, several reasons that it could alternatively be attributed to the ν_3 stretching mode of linear C_7S. First, as shown in Figure 4b, this peak, whose intensity is much larger than that of the ν_4 mode of the 12-**13**-**13**-12-12-12 C_6 isotopomer, appears among the products from an ablated $^{12}C/^{32}S$ mixture. Second, if this band were only produced by the ν_4 mode of a $^{12/13}C$ isotopomer, its intensity should be similar under the same experimental conditions. However, even though the same $^{12}C/^{13}C$ ratio was used in the mixture, the intensity of the 1913.6 cm^{-1} band is dramatically higher (cf. Figure 4a). We therefore assign the 1913.6 cm^{-1} band to the ν_3 stretching mode of linear C_7S.

Comparisons of observed and calculated isotopomer frequencies of the ν_3 mode for all-^{12}C, singly-^{13}C substituted, and all-^{13}C substituted $^{12/13}C_7S$ linear carbon−sulfur clusters are shown in Table 5. The deviation of calculated and experimental values varies only from −1.4 to +1.3 cm^{-1}, which indicates the reliability of these new assignments. This is confirmed by the good agreement of the isotopic shifts computed at different computational levels.

Although it is easy in theory to distinguish between two close-lying vibrational frequencies, this is usually difficult in practice. In some cases more than one isotopomer may contribute to a band envelope. For example, the 12-12-**13**-12-12-12-12-32 isotopomer (1913.0 cm^{-1}, cf., Table 5) is predicted to lie within the envelope of the total ^{12}C isotopomer observed at 1913.6 cm^{-1}. Furthermore, the net absorption of the singly-^{13}C-substituted isotopomer is usually larger than that of a doubly-^{13}C-substituted peak. Figure 2 makes clear that, after annealing, not only does the signal for the singly-^{13}C-substituted isotopomer get stronger but also the intensities for the doubly-^{13}C-substituted species are barely visible above the baseline. Because the calculated energy band separations for many doubly-^{13}C-substituted C_7S isotopomers are smaller than the $\nu_{exp} - \nu_{cal}$ energy differences, a reliable assignment of these bands becomes problematic.

Interestingly, the intensities of the $^{12/13}C_7$ isotopomer bands do not change during annealing. In previous work on pure

TABLE 4: Comparison of Observed (Ar Matrix, 35 K) and Calculated (B3LYP/6-311G* and B3LYP/cc-pVDZ) Isotopomer Frequencies (cm^{-1}) of the ν_2 Mode for All-^{12}C, Singly-^{13}C, and All-^{13}C Substituted $^{12/13}C_7S$ Linear Carbon−Sulfur Clusters

isotopomer	ν_{exp}[a]	$\nu_{6-311G*}$[b]	$\nu_{cc-pVDZ}$[c]	$\nu_{exp} - \nu_{6-311G*}$	$\nu_{exp} - \nu_{cc-pVDZ}$
12-12-12-12-12-12-12-32	2088.1	2088.1	2088.1	0.0	0.0
13-12-12-12-12-12-12-32	2088.1	2088.1	2087.8	0.0	0.3
12-**13**-12-12-12-12-12-32	2085.6	2087.4	2085.1	−1.8	0.5
12-12-**13**-12-12-12-12-32	2068.0	2067.3	2067.2	0.7	0.8
12-12-12-**13**-12-12-12-32	2060.5	2058.7	2060.2	1.8	0.3
12-12-12-12-**13**-12-12-32	2056.5	2056.5	2055.7	0.0	0.8
12-12-12-12-12-**13**-12-32	2063.6	2067.4	2063.7	−3.8	−0.1
12-12-12-12-12-12-**13**-32	2085.6	2087.0	2085.5	−1.4	0.1

[a] Tentative assignment. [b] Scaled by 0.9392 factor. [c] Scaled by 0.9452 factor.

TABLE 5: Comparison of Observed (Ar Matrix, 35 K) and Calculated (B3LYP/6-311G* and B3LYP/cc-pVDZ) Isotopomer Frequencies (cm^{-1}) of the ν_3 Mode for All-^{12}C, Singly-^{13}C, and All-^{13}C Substituted $^{12/13}C_7S$ Linear Carbon−Sulfur Clusters

isotopomer	ν_{exp}	$\nu_{6-311G*}$[a]	$\nu_{cc-pVDZ}$[b]	$\nu_{exp} - \nu_{6-311G*}$	$\nu_{exp} - \nu_{cc-pVDZ}$
12-12-12-12-12-12-12-32	1913.6	1913.6	1913.6	0.0	0.0
13-12-12-12-12-12-12-32	1904.7	1904.5	1904.7	0.2	0.0
12-**13**-12-12-12-12-12-32	1884.4	1885.5	1885.8	−1.1	−1.4
12-12-**13**-12-12-12-12-32	1913.6	1912.9	1913.0	0.7	0.6
12-12-12-**13**-12-12-12-32	1902.2	1901.9	1901.8	0.3	0.4
12-12-12-12-**13**-12-12-32	1911.7	1912.8	1912.8	−1.1	−1.1
12-12-12-12-12-**13**-12-32	1895.9	1896.5	1896.9	−0.6	−1.0
12-12-12-12-12-12-**13**-32	1902.2	1901.3	1901.3	0.9	0.9
13−**13**−**13**−**13**−**13**−**13**−**13**-32	1840.1	1838.8	1838.8	1.3	1.3

[a] Scaled by 0.9521 factor. [b] Scaled by 0.9480 factor.

TABLE 6: Comparison of Observed (Ar Matrix, 35 K) and Calculated (B3LYP/6-311G* and B3LYP/cc-pVDZ) Isotopomer Frequencies (cm^{-1}) of the ν_5 Mode for All-^{12}C, Singly-^{13}C, and All-^{13}C Substituted $^{12/13}C_7S$ Linear Carbon−Sulfur Clusters

isotopomer	ν_{exp}	$\nu_{6-311G*}$[a]	$\nu_{cc-pVDZ}$[b]	$\nu_{exp} - \nu_{6-311G*}$	$\nu_{exp} - \nu_{cc-pVDZ}$
12-12-12-12-12-12-12-32	1256.1	1256.1	1256.1	0.0	0.0
13-12-12-12-12-12-12-32	1246.9	1246.8	1246.8	0.1	0.1
12-**13**-12-12-12-12-12-32	1256.1	1256.1	1256.1	0.0	0.0
12-12-**13**-12-12-12-12-32	1246.3	1245.8	1245.8	0.5	0.5
12-12-12-**13**-12-12-12-32	1246.9	1246.5	1246.5	0.4	0.4
12-12-12-12-**13**-12-12-32	1256.1	1256.1	1256.1	0.0	0.0
12-12-12-12-12-**13**-12-32	1248.5	1248.3	1248.3	0.2	0.2
12-12-12-12-12-12-**13**-32	1245.0	1244.7	1244.6	0.3	0.4
13−**13**−**13**−**13**−**13**−**13**−**13**-32	1210.7	1210.2	1210.1	0.5	0.6

[a] Scaled by 0.9777 factor. [b] Scaled by 0.9739 factor.

carbon clusters,[36] it was found that the C_7 IR band also does not change upon annealing. This was interpreted to mean that the formation of C_7 from smaller carbon clusters and the reaction of C_7 to form larger clusters occurs with about equal rates. In the present case, if C_7S were formed from C_7 and S, it would be expected that the C_7 peaks would decrease due to this new reaction channel. Because no band intensity decrease was observed, we conclude that C_7S probably forms from smaller clusters such as C_nS and $C_{7-n}S$, $n = 1-6$; vide infra.

C. Isotopomer Band Assignments for the $\nu_5(\sigma)$ Vibration. Ablation and trapping of a $^{12}C/^{13}C$ mixture leads to only a single band in 1235−1260 cm^{-1} region, and this has been assigned to $^{12}C_{12}$ (cf. Figure 6c). For a $^{12}C/^{32}S$ mixture, only one peak at 1256.1 cm^{-1} is observed (cf. Figure 6b), which is here assigned to the ν_5 stretching mode of C_7S. With a mixture of $^{12}C/^{13}C/^{32}S$, a number of bands between 1245 and 1250 cm^{-1} are seen in addition to the strong band at 1256.1 cm^{-1} and another due to ^{13}CS. Assignments for these new peaks emerge from theoretical predictions of the isotopic shifts of linear C_7S. Table 6 lists all the observed and calculated isotopomer ν_5 mode frequencies of all-^{12}C, singly-^{13}C, and all-^{13}C substituted linear $^{12/13}C_7S$ clusters. The experimental frequencies are consistent with the predicted ones from different theoretical levels, with discrepancies of not more than 0.6 cm^{-1}. The ν_5 frequencies of the 12-**13**-12-12-12-12-12-32, and 12-12-12-12-**13**-12-12-32 isotopomers are exactly the same as that of the all-^{12}C isotopomer observed at 1256.1 cm^{-1}. As can be seen in Figure 1, this results from the fact that this vibrational mode has a node at the position of the ^{13}C substitutional site in these two isotopomers.

Figure 7 shows that the absorbance of the ν_5 mode (for all-^{12}C and singly-^{13}C substituted isotopomers) increases with temperature during annealing. The simultaneous decrease in the ^{13}CS absorption peak may be associated with the formation of C_7S. Although there is no direct information on how C_7S forms in the matrix, B3LYP/cc-pVDZ calculations show that the lowest energy pathway to C_7S occurs via reaction of C_6 and CS. Because $(CS)_2$ dimers have been reported in Ar matrices,[11] the CS moiety is probably mobile in solid Ar. The CS fragment is known to take part in the production of some C_nS clusters,[12] so it is reasonable to assume that CS may be a precursor for linear C_7S. Other formation channels are, however, also possible and could involve the mobile C and S species.

VI. Conclusions

$^{12/13}C_7S$ carbon−sulfur clusters have been produced by laser ablation of mixtures of graphite and sulfur, trapped in solid Ar at 12 K, and studied with FT-IR absorption spectroscopic methods. Theoretical calculations at different levels of theory show that C_7S is linear in Ar matrices. Newly observed IR absorption bands at 2088.1, 1913.6, and 1256.1 cm^{-1} have been assigned to ν_2, ν_3, and ν_5 C—C stretching modes of linear C_7S, respectively. The mechanism of formation of linear C_7S is most likely a simple addition reaction of C, CS, and S species to already-formed carbon−sulfur C_nS and pure carbon C_n clusters in the matrix.

Acknowledgment. We gratefully acknowledge the donors of the Petroleum Research Foundation, administered by the American Chemical Society, and the National Aeronautics and Space Administration for their support of this research.

References and Notes

(1) Meikle, W. P. S.; Allen, D. A.; Spyromilio, J.; Varani, G. F. *MNRAS* **1989**, *238*, 193.
(2) Cernicharo, J.; Guelin, M.; Hein, H.; Kahane, C. *Astron. Astrophys.* **1987**, *181*, L119.
(3) Yamamoto, S.; Saito, S.; Kawaguchi, K.; Kaifu, N.; Suzuki, H.; Ohishi, M. *Astrophys. J.* **1987**, *317*, L119.
(4) Bell, M. B.; Avery, L. W.; Feldman, P. A. *Astrophys. J.* **1993**, *417*, L37-L40.
(5) Spiro, C. L.; Banholtzer, W. F.; McAtee, D. S. *Thin Solid Films* **1992**, *220*, 122.
(6) Maier, G.; Schrot, J.; Reisenauer, H. P.; Janoschek, R. *Chem. Ber.* **1990**, *123*, 1753.
(7) Maier, G.; Reisenauer, H. P.; Schrot, J.; Janoschek, R. *Angew. Chem., Int. Ed. Engl.* **1990**, *29*, 1464.
(8) Maier, G.; Schrot, J.; Reisenauer, H. P. *Chem. Ber.* **1991**, *124*, 2613.
(9) Maier, G.; Schrot, J.; Reisenauer, H. P.; Janoschek, R. *Chem. Ber.* **1991**, *124*, 2617.
(10) Sulze, D.; Beye, N.; Fanghanel, E.; Schwarz, H. *Chem. Ber.* **1990**, *123*, 2069.
(11) Bohn, R. B.; Hannachi, Y.; Andrews, L. *J. Am. Chem. Soc.* **1992**, *114*, 6452.
(12) Szczepanski, J.; Hodyss, R.; Fuller, J.; Vala, M. *J. Phys. Chem. A* **1999**, *103*, 2975 and references therein.
(13) Saito, S.; Kawaguchi, K.; Yamamoto, S.; Ohishi, M.; Suzuki, H.; Kaifu, N. *Astrophys. J.* **1987**, *317*, L115.
(14) Yamamoto, S.; Saito, S.; Kawaguchi, K.; Kaifu, N.; Suzuki, H.; Ohishi, M. *Astrophys. J.* **1987**, *317*, L119.
(15) Hirahara, Y.; Oshima, Y.; Endo, Y. *Astrophys. J.* **1993**, *408*, L113.
(16) Kasai, Y.; Obi, K.; Oshima, Y.; Hirahara, Y.; Endo, Y.; Kawagushi, K.; Murakami, A. *Astrophys. J.* **1993**, *410*, L45.
(17) Gordon, V. D.; McCarthy, M. C.; Apponi, A. J.; Thaddeus, P. *Astrophys. J. Suppl. S* **2001**, *134*, 311.
(18) Peeso, D. J.; Ewing, D. W.; Curtis, T. T. *Chem. Phys. Lett.* **1990**, *166*, 307.
(19) Maurakami, A. *Astrophys. J.* **1990**, *357*, 288.
(20) Xie, Y.; Schaefer, H. F., III. *J. Chem. Phys.* **1992**, *96*, 3714.
(21) Cai, Z. L.; Zhang, X. G.; Wang, X. Y. *Chem. Phys. Lett.* **1990**, *213*, 168.
(22) Seeger, S.; Botschwina, P.; Flugge, J.; Reisenauer, H. P.; Maier, G. *J. Mol. Struct.* **1994**, *303*, 213.
(23) Martin, J. M. L.; Francois, J. P.; Gijbels, R. *J. Mol. Spectrosc.* **1995**, *169*, 445.
(24) Lee, S. *Chem. Phys. Lett.* **1997**, *268*, 69.
(25) Kim, K. H.; Lee, B.; Lee, S. *Chem. Phys. Lett.* **1998**, *297*, 65.
(26) Pascoli, G.; Lavendy, H. *Int. J. Mass Spectrom.* **1998**, *181*, 11.
(27) Fisher, K.; Hopwood, F.; Dance, I.; Willett, G. *New J. Chem.* **1999**, *23*, 609.
(28) Pascoli, G.; Lacendy, H. *Int. J. Mass Spectrom.* **2001**, *206*, 153.
(29) Tang, Z. C.; BelBruno, J. J. *Int. J. Mass Spectrom.* **2001**, *208*, 7.

(30) Frisch, M. J.; Trucks, G. W.; Schlegel, H. B.; Scuseria, G. E.; Robb, M. A.; Cheeseman, J. R.; Zakrzewski, V. G.; Montgomery, J. A., Jr.; Stratmann, R. E.; Burant, J. C.; Dapprich, S.; Millam, J. M.; Daniels, A. D.; Kudin, K. N.; Strain, M. C.; Farkas, O.; Tomasi, J.; Barone, V.; Cossi, M.; Cammi, R.; Mennucci, B.; Pomelli, C.; Adamo, C.; Clifford, S.; Ochterski, J.; Petersson, G. A.; Ayala, P. Y.; Cui, Q.; Morokuma, K.; Malick, D. K.; Rabuck, A. D.; Raghavachari, K.; Foresman, J. B.; Cioslowski, J.; Ortiz, J. V.; Baboul, A. G.; Stefanov, B. B.; Liu, G.; Liashenko, A.; Piskorz, P.; Komaromi, I.; Gomperts, R.; Martin, R. L.; Fox, D. J.; Keith, T.; Al-Laham, M. A.; Peng, C. Y.; Nanayakkara, A.; Gonzalez, C.; Challacombe, M.; Gill, P. M. W.; Johnson, B.; Chen, W.; Wong, M. W.; Andres, J. L.; Gonzalez, C.; Head-Gordon, M.; Replogle, E. S.; Pople, J. A. *Gaussian98*, revision A.3; Gaussian, Inc.: Pittsburgh, PA, 1998.

(31) Dunning, T. H., Jr. *J. Chem. Phys.* **1989**, *90*, 1007.

(32) Stanton, J. F.; Gauss, J.; Watts, J. D.; Nooijen, M.; Oliphant, N.; Perera, S. A.; Szalay, P. G.; Lauderdale, W. J.; Kucharski, S. A.; Gwaltney, S. R.; Beck, S.; Balková A.; Bernholdt, D. E.; Baeck, K. K.; Rozyczko, P.; Sekino, H.; Hober, C.; Bartlett, R. J. ACES II is a program product of the Quantum Theory Project, University of Florida.

(33) Kranze, R. H.; Graham, W. R. M. *J. Chem. Phys.* **1993**, *98*, 71.

(34) Kranze, R. H.; Rittby, C. M. L.; Graham, W. R. M. *J. Chem. Phys.* **1996**, *105*, 5313.

(35) Banisaukas, J.; Szczepanski, J.; Vala, M. Manuscript in preparation.

(36) Szczepanski, J.; Pellow, R.; Vala, M. *Z. Naturforsch.* **1991**, *47a*, 595.